

# Putting Flat $\Lambda$ CDM In The (Redshift) Bin

E. Ó Colgáin,<sup>1</sup> M. M. Sheikh-Jabbari,<sup>2,3</sup> R. Solomon,<sup>4</sup> M. G. Dainotti,<sup>5,6,7</sup> and D. Stojkovic<sup>4</sup>

<sup>1</sup>*CQuEST & Department of Physics, Sogang University, Seoul 121-742, Korea*

<sup>2</sup>*School of Physics, Institute for Research in Fundamental Sciences (IPM),*

*P.O.Box 19395-5531, Tehran, Iran*

<sup>3</sup>*The Abdus Salam ICTP, Strada Costiera 11, I-34014, Trieste, Italy*

<sup>4</sup>*HEPCOS, Department of Physics, SUNY at Buffalo, Buffalo, NY 14260-1500, USA*

<sup>5</sup>*National Astronomical Observatory of Japan, 2 Chome-21-1 Osawa, Mitaka, Tokyo 181-8588, Japan*

<sup>6</sup>*The Graduate University for Advanced Studies, SOKENDAI,*

*Shonankokusaimura, Hayama, Miura District, Kanagawa 240-0193, Japan*

<sup>7</sup>*Space Science Institute, Boulder, CO, USA*

Flat  $\Lambda$ CDM cosmology is specified by two constant fitting parameters in the late Universe, the Hubble constant  $H_0$  and matter density (today)  $\Omega_m$ . Through fitting  $(H_0, \Omega_m)$  to mock  $\Lambda$ CDM simulations in redshift bins, we confirm that  $A := H_0^2(1 - \Omega_m)$  and  $B := H_0^2\Omega_m$  distributions *spread* and *contract*, respectively, with increasing bin redshift. Noting that  $A = H_0^2 - B$ , the spread in  $A$  and contraction in  $B$  corresponds to a spread in  $H_0$ , and consequently in  $\Omega_m$ . Restricted to non-negative energy densities,  $A, B \geq 0$ , the spread in  $A$  yields a ‘pile up’ around  $A = 0$  or  $\Omega_m = 1$ . At even higher redshifts, further spreading flattens  $A$  and causes pile up near  $\Omega_m = 0$ . Thus, in generic higher redshift bins the Planck value  $\Omega_m \sim 0.3$  appears with low probability. We explore if observational Hubble data, Type Ia supernovae and standardisable quasars substantiate the features. We confirm that observed data exhibit an increasing  $\Omega_m$  (decreasing  $H_0$ ) trend with increasing bin redshift and that such behaviour can arise randomly within the flat  $\Lambda$ CDM model with probability  $p = 0.0021$  ( $3.1\sigma$ ).

## INTRODUCTION

Cosmologists are currently debating tensions within the flat  $\Lambda$ CDM cosmology; the two most serious concern the Hubble constant  $H_0$  and the  $S_8 \propto \sqrt{\Omega_m}$  parameter [1, 2]. These tensions have been framed as disagreements between the early (high redshift) and late (low redshift) Universe [3]. In particular, local  $H_0$  values [4–8] are universally biased to larger values than Planck- $\Lambda$ CDM [9]. Observations at different redshifts have shown that  $H_0$  evolves with effective (binned) redshift in the flat  $\Lambda$ CDM model [10–17] (see also [18]). If true, this behaviour is indicative of model breakdown [19, 20].

The flat  $\Lambda$ CDM model Hubble parameter  $H(z)$  is specified by two constant fitting parameters  $(H_0, \Omega_m)$  or  $(A, B)$ ,

$$\begin{aligned} H(z)^2 &= H_0^2 \left[ 1 - \Omega_m + \Omega_m(1+z)^3 \right], \\ &= A + B(1+z)^3. \end{aligned} \quad (1)$$

The term  $A$  is attributed to dark energy (DE), while the matter sector  $B$  scales as  $(1+z)^3$  and  $\Omega_m$  is bounded,  $0 \leq \Omega_m \leq 1$ . One can relax this constraint by allowing negative energy densities. Observe that DE becomes irrelevant at higher redshifts, where  $A \ll B(1+z)^3$  for reasonable values of  $\Omega_m$ . On the other hand, note that at higher redshifts  $H(z)^2 \sim B(1+z)^3$ , so the combination  $\Omega_m h^2$ , with  $h := H_0/100$ , is the relevant quantity. Exploiting these facts, it was recently argued that increases in  $\Omega_m$  (decreases in  $H_0$ ) with effective redshift are inherent to the flat  $\Lambda$ CDM model [16]. Here, we demonstrate through  $\Lambda$ CDM mocks binned by redshift that the probability of Planck values  $\Omega_m \sim 0.3$  decreases as we increase bin redshift. As a result, some evolution away from  $\Omega_m \sim 0.3$  should be expected in best fits of purely high redshift observations.

Armed with this analytic insight, we turn to observed data in order to ascertain whether the same trend exists through

comparison to mock simulations. We employ observational Hubble data (OHD), essentially cosmic chronometers [22] and baryon acoustic oscillations (BAO) [23, 24], Type Ia supernovae (SN) [25] and standardisable quasar (QSO) data sets [26]. Throughout we compare values of  $(H_0, \Omega_m)$  to mock simulations in the *same* redshift range, where the base cosmology for the mock is fixed by the best fit parameters of the *entire* data set. This allows us to confirm evolution between low and high redshifts in the sample.

Ultimately, while the fit of the overall sample to flat  $\Lambda$ CDM is largely dictated by the redshift range with greater density of data points, we will see that in sparser redshift ranges the data prefers discrepant cosmological parameters. In particular, we find probabilities as low as  $p = 0.021$  (OHD),  $p = 0.081$  (SN) and  $p = 0.019$  (QSOs), respectively, that mock data leads to similar values of  $(H_0, \Omega_m)$  as observed data. Combining the independent probabilities using Fisher’s method, one arrives at the probability  $p = 0.0021$  ( $3.1\sigma$ ) that such an evolution indeed exists within flat  $\Lambda$ CDM. An explanation in terms of selection biases is plausible for SN, e. g. [13, 15], but similar effects must impact cosmic chronometers, BAO, etc. Our mock analysis shows that *without selection biases* evolution away from Planck values should be expected.

## MOCK DATA

Consider now a simple data fitting exercise, where one takes Dark Energy Spectroscopic Instrument (DESI) forecasts for  $H(z)$  errors  $\sigma_{H(z_i)}$  at redshifts  $z_i$  in the range  $0.05 \leq z_i \leq 3.55$  [21]. Next, adopt Planck values [9],  $H_0 = 67.36$ ,  $\Omega_m = 0.315$ , for an underlying model and generate  $H(z_i)$  values in a normal distribution about the Planck- $\Lambda$ CDM model using the errors  $\sigma_{H(z_i)}$  as the standard deviation at each  $z_i$ . For

each realisation of mock data, separate the data into four bins, concretely  $0 < z < 0.8$ ,  $0.8 \leq z < 1.5$ ,  $1.5 \leq z < 2.3$  and  $2.3 \leq z < 3.6$ . This ensures similar data quality in each bin. Finally, fit the parameters  $(H_0, \Omega_m)$  from (1) to the data in each bin with a Gaussian prior on  $\Omega_m h^2 = 0.1430 \pm 0.0011$  [9]. Note that the prior only provides guidance for the high redshift behaviour of  $H(z)$  and its omission cannot change results (see appendix). Repeat the process a few thousand times and record the distribution of best fit values of  $(H_0, \Omega_m)$  for each bin.

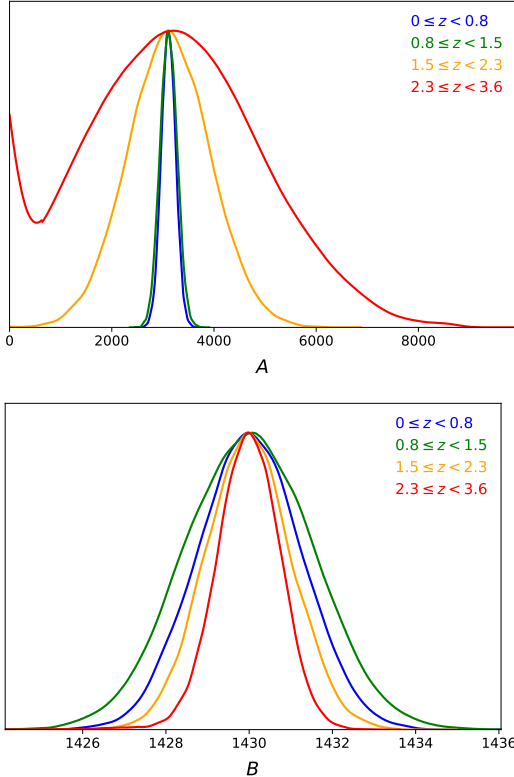


FIG. 1: Distributions of  $A = H_0^2(1 - \Omega_m)$  and  $B = H_0^2\Omega_m$  parameters reconstructed from mock simulations of the Planck-flat- $\Lambda$ CDM model in different redshift bins.

Before turning our attention to  $H_0, \Omega_m$  best fit distributions, let us report on the (unnormalised) distributions for  $A, B$ . Fig. 1, produced with *GetDist* [27], demonstrates that both  $A$  and  $B$  are Gaussian by inspection, except where  $A$  is impacted by the boundary at  $A = 0$ . Observe that the distributions in  $A$  and  $B$  spread and contract, respectively, with increasing bin redshift [61]. We have checked that  $A$  and  $B$  are uncorrelated, as may be expected. We also see that  $A$  grows a non-Gaussian tail around the  $A = 0$  ( $\Omega_m = 1$ ) region at higher redshift bins. This comes about, as a Gaussian with a wide spread probes the  $A < 0$  region with a growing probability at higher  $z$  bins, which we have dubbed a ‘pile up’ feature. Moreover, the width of the Gaussian distribution for  $B = H_0^2\Omega_m$  reduces as we go to higher redshift bins and hence we know  $B$  with a better precision in the higher redshift bins. Higher redshift spread in

$A = H_0^2 - B$  then yields spread in both  $H_0$  and  $\Omega_m$  values.

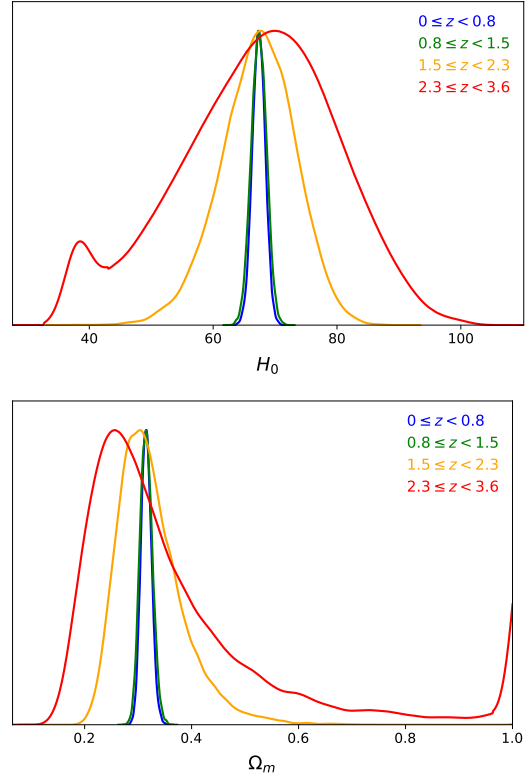


FIG. 2: Distributions of the cosmological parameters in different redshift bins. The ‘pile up’ at  $\Omega_m \sim 1$  and  $H_0 \sim 37.8$  km/s/Mpc is due to a build up of configurations at the physical bound  $\Omega_m = 1$ .

In Fig. 2 we show the same distribution in  $(H_0, \Omega_m)$  parameters. It is evident that both  $H_0$  and  $\Omega_m$  develop long non-Gaussian tails in the direction of lower  $H_0$  and larger  $\Omega_m$  despite input Planck values in the mocking procedure, confirming our analytic expectations discussed above. Recalling that  $\Omega_m h^2$  is constrained ( $B$  has a narrow Gaussian), the pile up around  $\Omega_m \sim 1$ , yields a peak at  $H_0 \sim \sqrt{1430} \sim 37.8$  km/s/Mpc. If one continues this analysis to even higher  $z$  bins, as we detail in the appendix, further flattening of  $A$  distribution leads to secondary effect with new peaks in the distribution around  $\Omega_m = 0$ . This is evident in Fig. 2 as the input value peak moves to the left. Observe that allowing for negative DE density,  $\Omega_m \leq 1$  or  $A \geq 0$ , allows  $A$  to spread unhindered to lower values, thereby removing pile up at  $\Omega_m = 1$ , but replacing it with pile up at  $H_0 = 0$ .

Since our mocking procedure is the same in each bin, while data quality does not change greatly (see [21]), one concludes that the behaviour is generic to the flat  $\Lambda$ CDM model. Note also that selection biases do not impact mocks. Moreover, the same argument can be run for *any* mock input parameters  $(H_0, \Omega_m)$ . Thus, one expects best fit  $\Omega_m$  parameters in higher redshift bins for observed data to pile up at  $\Omega_m \sim 1$ , and later  $\Omega_m \sim 0$ , but not at the Planck value  $\Omega_m \sim 0.3$ .

## OBSERVED DATA

Having uncovered a general feature of the flat  $\Lambda$ CDM model, we now look for the expected behaviour in real data.

### OHD

Here, we make use of cosmic chronometer [28–34] and BAO data [35–44]. More precisely, we work with the  $H(z)$  BAO determinations compiled in Table 2 of [45], where observations have been homogenised to be consistent with a uniform Planck inference of the sound horizon [46]. We added the newer constraint from eBOSS Quasar [47, 48], which we appropriately adjusted for the sound horizon,  $H(z = 1.48) = 153.59 \pm 8.27$ . Moreover, we have checked that replacing earlier Lyman- $\alpha$  BAO [42–44] with the latest constraints [49] does not change the results, so we work with the earlier determinations collated in [45].

First, we identify the best fit values of the cosmological parameters for the full sample,  $(H_0, \Omega_m) = (69.11, 0.299)$ , where it is worth noting that  $\Omega_m h^2 = 0.1428$ , consistent with the prior. Next, we repeat the mocking and binning procedure outlined earlier with the new input parameters  $(H_0, \Omega_m) = (69.11, 0.299)$ . Following [16] we impose a low redshift cut-off and isolate high redshift bins. In each bin we compare the best fit values from the real data and flat  $\Lambda$ CDM mocks in order to establish the probability of recovering *the same or larger*  $\Omega_m$  and *the same or smaller*  $H_0$  values. In the event of saturation of the bound  $\Omega_m = 1$ , this means that our probabilities are over-estimated, since allowing  $\Omega_m > 1$  permits further ordering of the values piled up at  $\Omega_m = 1$ . The results are shown in Table I, where it is clear that  $(H_0, \Omega_m)$  are evolving in the real data. Understandably, the probability of recovering similar values from mocks decreases with redshift up to a point where statistical fluctuations dominate and the probability increases again. Fig. 3 provides visual confirmation that despite the long tails, a bin exists where the real values are unexpected at  $\gtrsim 2\sigma$ . This points to redshift evolution in the sample, which should be expected given our discussions in the previous section.

$z$	$H_0$ (km/s/Mpc)	$\Omega_m$	Probability
$0.5 \leq z \leq 2.36$	69.68	0.294	0.646
$0.7 \leq z \leq 2.36$	65.67	0.331	0.326
$1 \leq z \leq 2.36$	61.27	0.380	0.258
$1.2 \leq z \leq 2.36$	53.91	0.491	0.120
$1.4 \leq z \leq 2.36$	41.55	0.828	0.037
$1.45 \leq z \leq 2.36$	37.80	1	0.021
$1.5 \leq z \leq 2.36$	37.80	1	0.069

TABLE I: Best fit cosmological parameters for different redshift ranges of OHD. Throughout, we impose the Planck prior,  $\Omega_m h^2 = 0.1430 \pm 0.0011$ . Flat  $\Lambda$ CDM simulations based on best fit parameters over the entire redshift range,  $0 < z \leq 2.33$ , allow us to establish the probability of higher  $\Omega_m$  and lower  $H_0$  values in real data. Where a discrepancy exists, we quote the largest probability.

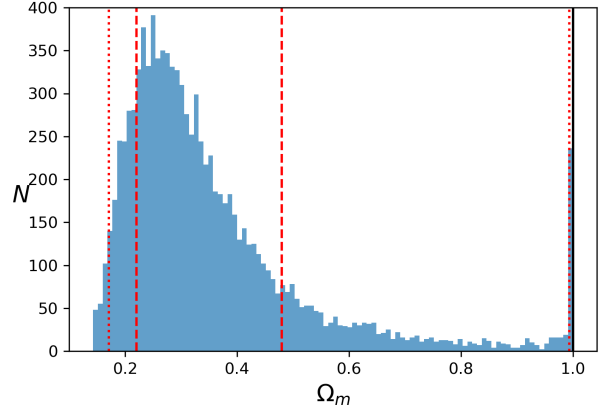


FIG. 3: Comparing 10,000 mock simulations with the best fit value of  $\Omega_m$  from OHD data (black line) for the bin  $1.45 \leq z \leq 2.36$ . Dashed and dotted lines denote the (2.3, 15.9, 84.1, 97.7) percentiles corresponding to  $1\sigma$  and  $2\sigma$  confidence intervals for a Gaussian distribution.

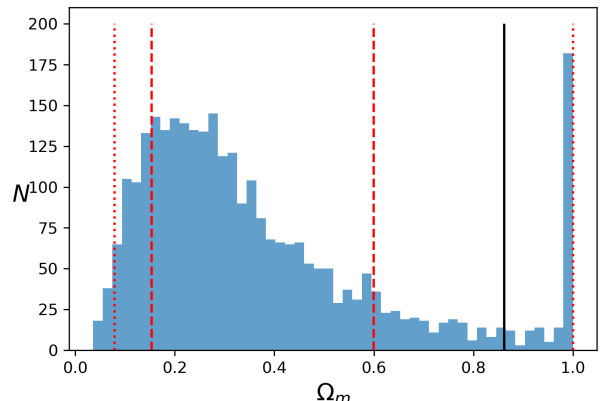


FIG. 4: Comparing 3,000 mock simulations with the best fit value of  $\Omega_m$  from SN data (black line) for the bin  $0.95 \leq z \leq 2.26$ . Dashed and dotted lines denote the (2.3, 15.9, 84.1, 97.7) percentiles corresponding to  $1\sigma$  and  $2\sigma$  confidence intervals for a Gaussian distribution.

### Type Ia SN

We revisit the analysis of the Pantheon data set [25] conducted in [16] (see also [13, 14]) in order to introduce a high redshift Planck prior on  $\Omega_m h^2$  [9]. Note, to do so, we treat the absolute magnitude of Type Ia SN  $M_B$  as a nuisance parameter. This gives SN data the freedom to adjust  $H_0$  so that the high redshift behaviour is always the same as Planck, otherwise the analysis is the same as before. We identify the best fit parameters  $(H_0, \Omega_m, M_B) = (69.26, 0.298, -19.37)$ , construct mock realisations in bins, which one compares to the real values. Throughout we allow for statistical and systematic uncertainties by cropping the Pantheon covariance matrix accordingly to fit the redshift bin. The results are shown in Table II

and Fig. 4, where the same trend as the OHD data is evident.

$z$	$H_0$ (km/s/Mpc)	$\Omega_m$	Probability
$0.7 < z \leq 2.26$	64.37	0.345	0.381
$0.8 < z \leq 2.26$	58.99	0.411	0.258
$0.9 < z \leq 2.26$	45.88	0.679	0.117
$0.95 < z \leq 2.26$	40.73	0.862	0.081
$1 < z \leq 2.26$	43.16	0.768	0.170

TABLE II: Same as Table I but for Pantheon SN. We treat the absolute magnitude  $M_B$  as an additional nuisance parameter when we fit mock realisations and real data. We quote the probability of larger values of  $\Omega_m$  and lower values of  $H_0$ . The additional freedom in  $M_B$  means that these probabilities always agree.

### Standardisable QSOs

Finally we turn our attention to QSOs standardised through the Risaliti-Lusso proposal [51, 52]. We refer readers to the original texts for methodology. Objectively, QSOs constitute emerging cosmological probes [53, 59] and are understandably less well developed than the SN and BAO; nevertheless, even now SN remain a work in progress [54]. In particular, there is considerable intrinsic scatter in the QSO data and there is an ongoing debate about the standardisability of the Risaliti-Lusso QSOs [56–60]. Nonetheless, QSOs support our narrative and this justifies their inclusion. In contrast to OHD and SN, which have lower error-weighted (effective) redshifts of  $z_{\text{eff}} \sim 0.5$  and  $z_{\text{eff}} \sim 0.3$ , respectively, the QSO sample [26] has a higher effective redshift  $z_{\text{eff}} \sim 1.4$ . Moreover, it is well documented that  $\Omega_m$  adopts larger values than expected at higher redshifts [52, 55] and that evolution happens within the QSO sample [16, 52]. The key point here is that any evolution of  $\Omega_m$  with effective redshift may be telling us less about QSOs and more about the flat  $\Lambda$ CDM model and hence

$z$	$H_0$ (km/s/Mpc)	$\Omega_m$	Probability
$0 < z \leq 0.3$	406.41	0.009	0.073
$0 < z \leq 0.5$	353.47	0.011	0.028
$0 < z \leq 0.55$	433.91	0.008	0.019
$0 < z \leq 0.6$	381.50	0.010	0.020
$0 < z \leq 0.7$	73.40	0.265	0.096
$0 < z \leq 0.8$	58.48	0.418	0.117
$0 < z \leq 1$	40.69	0.864	0.400

TABLE III: Same as Table I but for Risaliti-Lusso QSOs. We treat  $\beta$ ,  $\gamma$  and  $\delta$  (see [51] for definitions), as additional nuisance parameters when we fit mock realisations and real data. We quote the probability of *lower* values of  $\Omega_m$  and *higher* values of  $H_0$ .

Our analysis here follows the earlier sections, but there is a key difference. Risaliti-Lusso QSOs return best fits of  $\Omega_m \sim 1$  across the full sample [55–58], whereas at lower redshifts  $0 < z \lesssim 0.7$ , one recovers Planck values,  $\Omega_m \sim 0.3$  [16]; in accord with our earlier discussions and analyses. Thus, we start from the redshift range  $0 < z \leq 1.4$  (1326 QSOs), where  $\Omega_m$  hits the bound  $\Omega_m = 1$ , and identify the best fit

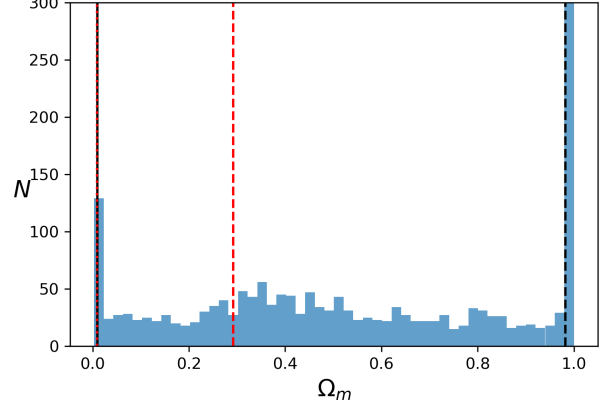


FIG. 5: A comparison between 3,000 mock simulations and the best fit value of  $\Omega_m$  from QSO data (black line) for the bin  $0 < z \leq 0.55$ . Dashed and dotted red lines denote the (2.3, 15.9) percentiles corresponding to  $1\sigma$  and  $2\sigma$  confidence intervals for a Gaussian distribution. The dashed black line denotes the median,  $\Omega_m = 0.982$ .

parameters that serve as inputs for mocks,  $(H_0, \Omega_m, \beta, \gamma, \delta) = (37.82, 1, 8.64, 0.61, 0.24)$ . To construct the mocks, we generate new UV fluxes  $F_{UV}$  by picking values in a normal distribution about the original values with a standard deviation set to the error. Next, we generate corresponding central values for the X-ray fluxes  $F_X$  through the relation [51, 52],

$$\log_{10} F_X = \beta + \gamma \log_{10} F_{UV} + (\gamma - 1) \log_{10}(4\pi D_L^2), \quad (2)$$

where  $D_L(z)$  is the luminosity distance, before displacing the values with the standard deviation  $\sqrt{\delta^2 + \sigma_i^2}$ , where  $\sigma_i$  is the error on  $\log_{10} F_{X,i}$  at redshift  $z_i$ .

In Table III we show the increasing (decreasing) trend of  $\Omega_m$  ( $H_0$ ) with effective redshift. Unexpectedly large values of  $H_0$  and small values of  $\Omega_m$  are driven partially by poor data quality and the Planck prior on  $\Omega_m h^2$ . Nevertheless, the trend in central values is the same and one notes that the probability of recovering the best fit values for real data decreases as the effective redshift of the bin decreases, confirming that the best fit values of the entire data set are less representative. In Fig. 5 we provide visual confirmation of this result in a given range, where it is notable that the  $\Omega_m$  distribution is uniform between the bounds, thus underscoring how poorly QSO data constrains  $\Omega_m$ . This is presumably due to the large scatter and fewer QSOs at lower redshifts.

### CONCLUSIONS

We explained through analytic arguments and simulations why the Planck value  $\Omega_m \sim 0.3$  is unlikely when one fits higher redshift binned observations to the flat  $\Lambda$ CDM model. Our arguments are independent of mock input parameters and simply follow from the irrelevance of the  $A$  term in (1) at higher redshifts, and  $A \geq 0$ , which yield an initial ‘pile up’

of best fits on  $\Omega_m = 1$ , before piling up at  $\Omega_m \sim 0$  at even higher redshifts. This reduces the probability of recovering the Planck value at high redshift, thus providing an avenue to test the model. One can of course believe  $\Omega_m \sim 0.3$ , but probability is not on one's side.

We have confirmed an increasing  $\Omega_m$  behaviour in OHD and Type Ia SN with  $p$ -values  $p = 0.021$  ( $2.3\sigma$ ) and  $p = 0.081$  ( $1.7\sigma$ ). Using Fisher's method, the combined probability for these established cosmological probes is  $p = 0.013$  ( $2.5\sigma$ ). In QSOs, an intrinsically high redshift observable, we see the opposite trend where discrepant best fit  $(H_0, \Omega_m)$  values relative to the entire sample appear at lower redshifts with  $p = 0.019$  ( $2.3\sigma$ ). Once again combining the probabilities, one finds  $p = 0.0021$  ( $3.1\sigma$ ). One may also benchmark with respect to the bin  $0 < z \leq 0.7$ , where  $\Omega_m \sim 0.3$ , in which case the combined probability becomes  $p = 0.0078$  ( $2.7\sigma$ ).

Regardless, all observables show signatures of evolution to higher values of  $\Omega_m$  between low and high redshifts, in line with our expectations that they can be displaced from Planck values. Neglecting selection effects, and more general systematics, across multiple observables (SN, cosmic chronometers, BAO, QSOs), this supports the idea that the flat  $\Lambda$ CDM model is a dynamical model where its fitting parameters, which should be constants, evolve in (cosmic) time. This cautions that cosmological tensions may be an outcome of the flawed assumption that  $(H_0, \Omega_m)$  are unique within flat  $\Lambda$ CDM.

**Acknowledgements** We thank Stephen Appleby, Eleonora Di Valentino, Adam Riess, Joe Silk and Jenny Wagner for correspondence. We also thank Bum-Hoon Lee, Wonwoo Lee, Albin Nilsson, Mehrdad Mirbabaei, Somyadip Thakur and Lu Yin for discussion. EOC was supported by the National Research Foundation of Korea grant funded by the Korea government (MSIT) (NRF-2020R1A2C1102899). DS is partially supported by the US National Science Foundation, under Grant No. PHY-2014021. MMSJ would like to acknowledge SarAmadan grant No. ISEF/M/400121 and ICTP HECAP section where this project was carried out. M.G. acknowledge the support of Division of Science at NAOJ.

## Appendix

### Appendix 1: Removing $\Omega_m h^2$ prior

Removing the Planck  $\Omega_m h^2$  prior from Fig. 2 leads to a spreading in all distributions, but qualitatively the features are the same, as expected from the analytic discussions. This can be confirmed in Fig. 6.

### Appendix 2: Confirmation of $P(\Omega_m \sim 0.3) \rightarrow 0$

In this section we consider the same mocking procedure but focus exclusively on the fourth DESI bin with redshift range  $2.3 \leq z < 3.6$ . We now displace the redshifts in intervals of  $\pm 1$  without changing the data and document the effect on the distribution of  $\Omega_m$  best fits over a few thousand mocks. Once

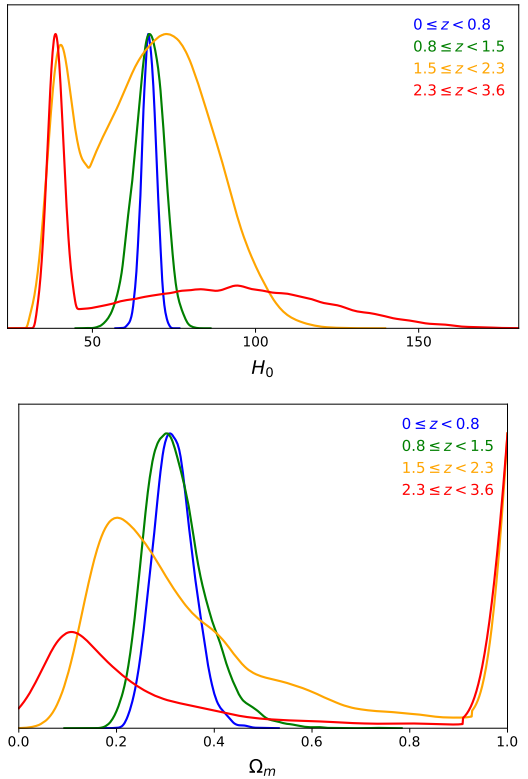


FIG. 6: Same as Fig. 2, but without the  $\Omega_m h^2$  prior.

again, we assume Planck input parameters,  $H_0 = 67.36$ ,  $\Omega_m = 0.315$  and the Gaussian prior,  $\Omega_m h^2 = 0.1430 \pm 0.0011$  [9]. In Fig. 7 we present (normalised) probabilities for  $\Omega_m$  for Planck- $\Lambda$ CDM mocks, where the blue curve corresponds to the red curve in Fig. 2. The remaining curves correspond to  $\Omega_m$  probabilities as we displace the original binned data in redshift. Since we are at high redshift, the probability of  $\Omega_m = 1$ ,  $P(\Omega_m = 1) > 0$  and it clearly increases with redshift of the sample. This corresponds to the  $A$  distribution spreading to smaller values, where it is impacted by the bound at  $A = 0$ . However,  $A$  must also spread to higher values, and since  $B := H_0^2 \Omega_m$  is fixed, in the sense that this combination is relevant at higher redshifts, the only way  $A = H_0^2 - B$  can spread to higher values is increasing  $H_0$  and decreasing  $\Omega_m$ . This spreading of the  $A$  distribution to larger values explains why the peaks in Fig. 2 get displaced from their input values. In Fig. 7 this trend is more pronounced and it is an obvious implication that at a given high redshift, any knowledge of the input parameters is lost and the probability of recovering the Planck value,  $P(\Omega_m \sim 0.3)$  is close to zero.

- 
- [1] E. Di Valentino, O. Mena, S. Pan, L. Visinelli, W. Yang, A. Melchiorri, D. F. Mota, A. G. Riess and J. Silk, *Class. Quant. Grav.* **38** (2021) no.15, 153001 [[arXiv:2103.01183](https://arxiv.org/abs/2103.01183) [astro-ph.CO]].
  - [2] E. Abdalla, G. Franco Abellán, A. Aboubrahim, A. Agnello,

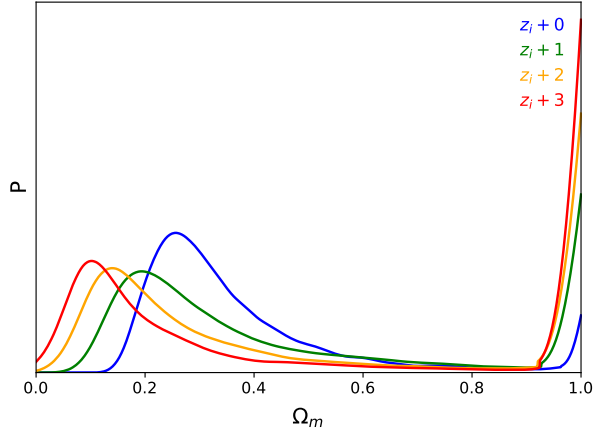


FIG. 7: Probabilities of a given  $\Omega_m$  best fit value for forecast DESI  $H(z)$  data in the range  $2.3 \leq z < 3.6$  (blue curve) with Planck input values. Green, yellow and red denote the probabilities if the same forecasted data quality is displaced to higher redshifts.

- O. Akarsu, Y. Akrami, G. Alestas, D. Aloni, L. Amendola and L. A. Anchordoqui, *et al.* JHEAp **34** (2022), 49-211 [[arXiv:2203.06142](#) [astro-ph.CO]].
- [3] L. Verde, T. Treu and A. G. Riess, Nature Astron. **3**, 891 [[arXiv:1907.10625](#) [astro-ph.CO]].
- [4] A. G. Riess, W. Yuan, L. M. Macri, D. Scolnic, D. Brout, S. Casertano, D. O. Jones, Y. Murakami, L. Breuval and T. G. Brink, *et al.* [[arXiv:2112.04510](#) [astro-ph.CO]].
- [5] W. L. Freedman, “Measurements of the Hubble Constant: Tensions in Perspective,” Astrophys. J. **919** (2021) no.1, 16 [[arXiv:2106.15656](#) [astro-ph.CO]].
- [6] D. W. Pesce, J. A. Braatz, M. J. Reid, A. G. Riess, D. Scolnic, J. J. Condon, F. Gao, C. Henkel, C. M. V. Impellizzeri and C. Y. Kuo, *et al.* “The Megamaser Cosmology Project. XIII. Combined Hubble constant constraints,” Astrophys. J. Lett. **891** (2020) L1 [[arXiv:2001.09213](#) [astro-ph.CO]].
- [7] E. Kourkchi, R. B. Tully, G. S. Anand, H. M. Courtois, A. Dupuy, J. D. Neill, L. Rizzi and M. Seibert, Astrophys. J. **896** (2020) no.1, 3 [[arXiv:2004.14499](#) [astro-ph.GA]].
- [8] J. P. Blakeslee, J. B. Jensen, C. P. Ma, P. A. Milne and J. E. Greene, Astrophys. J. **911** (2021) no.1, 65 [[arXiv:2101.02221](#) [astro-ph.CO]].
- [9] N. Aghanian *et al.* [Planck], Astron. Astrophys. **641** (2020), A6 [[arXiv:1807.06209](#) [astro-ph.CO]].
- [10] K. C. Wong, S. H. Suyu, G. C. F. Chen, C. E. Rusu, M. Millon, D. Sluse, V. Bonvin, C. D. Fassnacht, S. Taubenberger and M. W. Auger, *et al.* Mon. Not. Roy. Astron. Soc. **498** (2020) no.1, 1420-1439 [[arXiv:1907.04869](#) [astro-ph.CO]].
- [11] M. Millon, A. Galan, F. Courbin, T. Treu, S. H. Suyu, X. Ding, S. Birrer, G. C. F. Chen, A. J. Shajib and D. Sluse, *et al.* Astron. Astrophys. **639** (2020), A101 [[arXiv:1912.08027](#) [astro-ph.CO]].
- [12] C. Krishnan, E. Ó Colgáin, Ruchika, A. A. Sen, M. M. Sheikh-Jabbari and T. Yang, Phys. Rev. D **102** (2020) no.10, 103525 [[arXiv:2002.06044](#) [astro-ph.CO]].
- [13] M. G. Dainotti, B. De Simone, T. Schiavone, G. Montani, E. Rinaldi and G. Lambiase, Astrophys. J. **912** (2021) no.2, 150 [[arXiv:2103.02117](#) [astro-ph.CO]].
- [14] N. Horstmann, Y. Pietschke and D. J. Schwarz, [[arXiv:2111.03055](#) [astro-ph.CO]].

- [15] M. G. Dainotti, B. De Simone, T. Schiavone, G. Montani, E. Rinaldi, G. Lambiase, M. Bogdan and S. Ugale, Galaxies **10** (2022), 24 [[arXiv:2201.09848](#) [astro-ph.CO]].
- [16] E. Ó Colgáin, M. M. Sheikh-Jabbari, R. Solomon, G. Bar-giacchi, S. Capozziello, M. G. Dainotti and D. Stojkovic, [[arXiv:2203.10558](#) [astro-ph.CO]].
- [17] J. Wagner, [[arXiv:2203.11219](#) [astro-ph.CO]].
- [18] J. P. Hu and F. Y. Wang, [[arXiv:2203.13037](#) [astro-ph.CO]].
- [19] C. Krishnan, E. Ó Colgáin, M. M. Sheikh-Jabbari and T. Yang, Phys. Rev. D **103** (2021) no.10, 103509 [[arXiv:2011.02858](#) [astro-ph.CO]].
- [20] C. Krishnan and R. Mondol, [[arXiv:2201.13384](#) [astro-ph.CO]].
- [21] A. Aghamousa *et al.* [DESI], [[arXiv:1611.00036](#) [astro-ph.IM]].
- [22] R. Jimenez and A. Loeb, Astrophys. J. **573** (2002), 37-42 [[arXiv:astro-ph/0106145](#) [astro-ph]].
- [23] H. J. Seo and D. J. Eisenstein, Astrophys. J. **598** (2003), 720-740 [[arXiv:astro-ph/0307460](#) [astro-ph]].
- [24] D. J. Eisenstein *et al.* [SDSS], Astrophys. J. **633** (2005), 560-574 [[arXiv:astro-ph/0501171](#) [astro-ph]].
- [25] D. M. Scolnic *et al.* [Pan-STARRS1], Astrophys. J. **859** (2018) no.2, 101 [[arXiv:1710.00845](#) [astro-ph.CO]].
- [26] E. Lusso, G. Risaliti, E. Nardini, G. Bargiacchi, M. Benetti, S. Bisogni, S. Capozziello, F. Civano, L. Eggelston and M. Elvis, *et al.* Astron. Astrophys. **642** (2020), A150 [[arXiv:2008.08586](#) [astro-ph.GA]].
- [27] A. Lewis, [[arXiv:1910.13970](#) [astro-ph.IM]].
- [28] D. Stern, R. Jimenez, L. Verde, M. Kamionkowski and S. A. Stanford, JCAP **02** (2010), 008 [[arXiv:0907.3149](#) [astro-ph.CO]].
- [29] M. Moresco, A. Cimatti, R. Jimenez, L. Pozzetti, G. Zamorani, M. Bolzonella, J. Dunlop, F. Lamareille, M. Mignoli and H. Pearce, *et al.* JCAP **08** (2012), 006 [[arXiv:1201.3609](#) [astro-ph.CO]].
- [30] C. Zhang, H. Zhang, S. Yuan, T. J. Zhang and Y. C. Sun, Res. Astron. Astrophys. **14** (2014) no.10, 1221-1233 [[arXiv:1207.4541](#) [astro-ph.CO]].
- [31] M. Moresco, L. Pozzetti, A. Cimatti, R. Jimenez, C. Maraston, L. Verde, D. Thomas, A. Citro, R. Tojeiro and D. Wilkinson, JCAP **05** (2016), 014 [[arXiv:1601.01701](#) [astro-ph.CO]].
- [32] A. L. Ratsimbazafy, S. I. Loubser, S. M. Crawford, C. M. Cress, B. A. Bassett, R. C. Nichol and P. Väistönen, Mon. Not. Roy. Astron. Soc. **467** (2017) no.3, 3239-3254 [[arXiv:1702.00418](#) [astro-ph.CO]].
- [33] N. Borghi, M. Moresco and A. Cimatti, Astrophys. J. Lett. **928** (2022) no.1, L4 [[arXiv:2110.04304](#) [astro-ph.CO]].
- [34] K. Jiao, N. Borghi, M. Moresco and T. J. Zhang, [[arXiv:2205.05701](#) [astro-ph.CO]].
- [35] E. Gaztanaga, A. Cabre and L. Hui, Mon. Not. Roy. Astron. Soc. **399** (2009), 1663-1680 [[arXiv:0807.3551](#) [astro-ph]].
- [36] A. Oka, S. Saito, T. Nishimichi, A. Taruya and K. Yamamoto, Mon. Not. Roy. Astron. Soc. **439** (2014), 2515-2530 [[arXiv:1310.2820](#) [astro-ph.CO]].
- [37] Y. Wang *et al.* [BOSS], Mon. Not. Roy. Astron. Soc. **469** (2017) no.3, 3762-3774 [[arXiv:1607.03154](#) [astro-ph.CO]].
- [38] C. H. Chuang and Y. Wang, Mon. Not. Roy. Astron. Soc. **435** (2013), 255-262 [[arXiv:1209.0210](#) [astro-ph.CO]].
- [39] S. Alam *et al.* [BOSS], Mon. Not. Roy. Astron. Soc. **470** (2017) no.3, 2617-2652 [[arXiv:1607.03155](#) [astro-ph.CO]].
- [40] C. Blake, S. Brough, M. Colless, C. Contreras, W. Couch, S. Croom, D. Croton, T. Davis, M. J. Drinkwater and K. Forster, *et al.* Mon. Not. Roy. Astron. Soc. **425** (2012), 405-414 [[arXiv:1204.3674](#) [astro-ph.CO]].

- [41] L. Anderson, E. Aubourg, S. Bailey, F. Beutler, A. S. Bolton, J. Brinkmann, J. R. Brownstein, C. H. Chuang, A. J. Cuesta and K. S. Dawson, *et al.* Mon. Not. Roy. Astron. Soc. **439** (2014) no.1, 83-101 [[arXiv:1303.4666](#) [astro-ph.CO]].
- [42] J. E. Bautista, N. G. Busca, J. Guy, J. Rich, M. Blomqvist, H. d. Bourboux, M. M. Pieri, A. Font-Ribera, S. Bailey and T. Delubac, *et al.* Astron. Astrophys. **603** (2017), A12 [[arXiv:1702.00176](#) [astro-ph.CO]].
- [43] T. Delubac *et al.* [BOSS], Astron. Astrophys. **574** (2015), A59 [[arXiv:1404.1801](#) [astro-ph.CO]].
- [44] A. Font-Ribera *et al.* [BOSS], JCAP **05** (2014), 027 [[arXiv:1311.1767](#) [astro-ph.CO]].
- [45] J. Magana, M. H. Amante, M. A. Garcia-Aspeitia and V. Motta, Mon. Not. Roy. Astron. Soc. **476** (2018) no.1, 1036-1049 [[arXiv:1706.09848](#) [astro-ph.CO]].
- [46] P. A. R. Ade *et al.* [Planck], Astron. Astrophys. **594** (2016), A13 [[arXiv:1502.01589](#) [astro-ph.CO]].
- [47] J. Hou, A. G. Sánchez, A. J. Ross, A. Smith, R. Neveux, J. Bautista, E. Burtin, C. Zhao, R. Scoccimarro and K. S. Dawson, *et al.* Mon. Not. Roy. Astron. Soc. **500** (2020) no.1, 1201-1221 [[arXiv:2007.08998](#) [astro-ph.CO]].
- [48] R. Neveux, E. Burtin, A. de Mattia, A. Smith, A. J. Ross, J. Hou, J. Bautista, J. Brinkmann, C. H. Chuang and K. S. Dawson, *et al.* Mon. Not. Roy. Astron. Soc. **499** (2020) no.1, 210-229 [[arXiv:2007.08999](#) [astro-ph.CO]].
- [49] H. du Mas des Bourboux, J. Rich, A. Font-Ribera, V. de Sainte Agathe, J. Farr, T. Etourneau, J. M. Le Goff, A. Cuceu, C. Balland and J. E. Bautista, *et al.* Astrophys. J. **901** (2020) no.2, 153 [[arXiv:2007.08995](#) [astro-ph.CO]].
- [50] G. E. Addison, Y. Huang, D. J. Watts, C. L. Bennett, M. Halpern, G. Hinshaw and J. L. Weiland, Astrophys. J. **818** (2016) no.2, 132 [[arXiv:1511.00055](#) [astro-ph.CO]].
- [51] G. Risaliti and E. Lusso, Astrophys. J. **815** (2015), 33 [[arXiv:1505.07118](#) [astro-ph.CO]].
- [52] G. Risaliti and E. Lusso, Nature Astron. **3** (2019) no.3, 272-277 [[arXiv:1811.02590](#) [astro-ph.CO]].
- [53] M. Moresco, L. Amati, L. Amendola, S. Birrer, J. P. Blakeslee, M. Cantiello, A. Cimatti, J. Darling, M. Della Valle and M. Fishbach, *et al.* [[arXiv:2201.07241](#) [astro-ph.CO]].
- [54] C. Meldorf, A. Palmese, D. Brout, R. Chen, D. Scolnic, L. Kelsey, L. Galbany, W. Hartley, T. Davis and A. Drlica-Wagner, *et al.* [[arXiv:2206.06928](#) [astro-ph.CO]].
- [55] T. Yang, A. Banerjee and E. Ó Colgáin, Phys. Rev. D **102** (2020) no.12, 123532 [[arXiv:1911.01681](#) [astro-ph.CO]].
- [56] N. Khadka and B. Ratra, Mon. Not. Roy. Astron. Soc. **497** (2020) no.1, 263-278 [[arXiv:2004.09979](#) [astro-ph.CO]].
- [57] N. Khadka and B. Ratra, Mon. Not. Roy. Astron. Soc. **502** (2021) no.4, 6140-6156 [[arXiv:2012.09291](#) [astro-ph.CO]].
- [58] N. Khadka and B. Ratra, Mon. Not. Roy. Astron. Soc. **510** (2022) no.2, 2753-2772 [[arXiv:2107.07600](#) [astro-ph.CO]].
- [59] M. G. Dainotti, V. Nielson, G. Sarracino, E. Rinaldi, S. Nagataki, S. Capozziello, O. Y. Gnedin and G. Bargiacchi, [[arXiv:2203.15538](#) [astro-ph.CO]].
- [60] V. Petrosian, J. Singal and S. Mutchnick, [[arXiv:2205.07981](#) [astro-ph.CO]].
- [61] Interestingly the distribution in  $B$  spreads from bin 1 to bin 2 before contracting in bins 3 and 4.